Extraction of Glacial Lake Outlines in Tibet Plateau Using Landsat 8 Imagery and Google Earth Engine

Fang Chen, Meimei Zhang, Bangsen Tian, and Zhen Li, *Member, IEEE*

***Abstract*—Glacial lake outburst floods (GLOFs) are among the most serious natural hazards in high mountain regions in the last several decades. The recent global warming has caused dramatic glacial lake changes and increased potential GLOF risk, particularly in Tibet Plateau (TP). Thus there is a pressing need to understand area and spatial distribution of glacial lakes at a large scale. Current efforts about glacial lake mapping in TP region is limited by spurious detections in the heterogeneous backgrounds. The nonlocal active contour algorithm, which takes full consideration of the regional heterogeneity in image, has been effectively applied in the field of medical image segmentation, but has not been tested at large scale of glaciated area yet. Moreover, the improved radiometric resolution and geographic coverage from Landsat 8 provides an opportunity to map glacial lakes. This study evaluated the potential of Landsat 8 images on annual glacial lake mapping in TP region which was characterized by various complex water conditions. The Google Earth Engine based cloud computing effectively facilitated the processing of a complete time series of Landsat 8 imagery from 2015 (156 path/rows and approximately 3580 scenes). Characteristics of glacial lake distribution were analyzed from aspects of size classes and elevation. Our results demonstrate that these strategies and methods automatically produce highly reliable glacial lake extents across the entire TP region, and are potentially applicable to other large-scale glacial lake mapping projects.**

***Index Terms*—Glacial lake, Google Earth Engine, Landsat 8, non-local active contour, Tibet Plateau.**

I. Introduction

IT is widely known that glaciers serve as a sensitive indicator of terrestrial climate and environmental changes as well as important water resources in mountainous areas. In response to climate warming, the majority of glaciers on the Tibetan Plateau are now retreating and thinning, not only affects meltwater availability [1], runoff regimes [2] and hydrological processes [3] in the region but also accelerate glacial lake evolution and increase the risk of glacial lake outburst floods (GLOFs). GLOFs are of high scientific importance because they can suddenly cause catastrophic damages and fatalities in the downstream regions [4], [5]. Mapping and monitoring these glacial lakes would improve our understanding of regional climate change and potential hazards.

Glacial lakes are typically located in remote areas and spaceborne remote sensing provides a feasible technique for systematic glacial lake mapping and inventory at a large scale. The Landsat series of satellites provide the longest temporal and spatial record for earth surface observation since their first launch in 1972. The recently launched Landsat 8 on February 11, 2013 is expected to extend the Landsat mission into the next decade. In addition to improved performance in terms of radiometric resolution and high signal-to-noise ratios (SNR), an improved duty cycle allows collection of a significantly greater number of images per day, particularly at the equator and higher latitude areas [6]–[8], thus providing more data sources for climate change studies, and have been widely used in glacial lake mapping and other researches of cryospheric sciences. The spatial distribution and temporal changes of glacial lakes were investigated by manual digitization for the High Mountain Asia using Landsat data [5]. Many studies commonly use two-band spectral water indices such as Normalized Difference Water Index (NDWI) [9] and modified NDWI (MNDWI) [10] to derive glacial lake extent by setting a single threshold [11]–[13]. An automated algorithm was developed based on the histogram of NDWI and applied to delineate glacial lakes from Landsat images in circa 1990, 2000 and 2009 across the Himalaya mountains [14]. Apart from water indices, many features such as multispectral bands, texture and mid-level or high-level features learned by deep neural networks could also be used as the inputs of image segmentation [15]. Thermal infrared analysis is another way to investigate temperature differences in glacial lakes for the further automated detection [16], [17].

Although these efforts have greatly increase the knowledge on the distribution of glacial lakes and their development from spatial and temporal domains, these studies are limited by significant amount of manual interpretation and editing. Besides, in the case of glacial lakes that are abundant at small sizes, because of the characteristics of the source glacier and lake bed, and due to the water depth and sediment influx, these lakes appear

Manuscript received January 13, 2017; revised March 28, 2017 and May 2, 2017; accepted May 15, 2017. Date of publication June 5, 2017; date of current version September 20, 2017. This research was supported by the study on the spatial and temporal scaling conversion method of remote sensing evapotranspiration within the water balance constraints, the National Natural Science Foundation Project (41401511) and the Constructions detection and damage evaluation model after earthquake based on multi-task transfer learning, the National Natural Science Foundation Project (41601451). *(Corresponding author: Meimei Zhang.)*

F. Chen is with the Key Laboratory of Digital Earth Science, Institute of Remote Sensing and Digital Earth, Chinese Academy of Sciences, Beijing 100094, China, the Hainan Key Laboratory of Earth Observation, Institute of Remote Sensing and Digital Earth, Chinese Academy of Sciences, Sanya 572029, China, and also with the University of Chinese Academy of Sciences, Beijing 100049, China (e-mail: chenfang_group@radi.ac.cn).

M. Zhang, B. Tian, and Z. Li are with the Key Laboratory of Digital Earth Science, Institute of Remote Sensing and Digital Earth, Chinese Academy of Sciences, Beijing 100094, China (e-mail: zhangmm@radi.ac.cn; tianbs@radi.ac.cn; lizhen@radi.ac.cn).

Color versions of one or more of the figures in this paper are available online at http://ieeexplore.ieee.org.

Digital Object Identifier 10.1109/JSTARS.2017.2705718

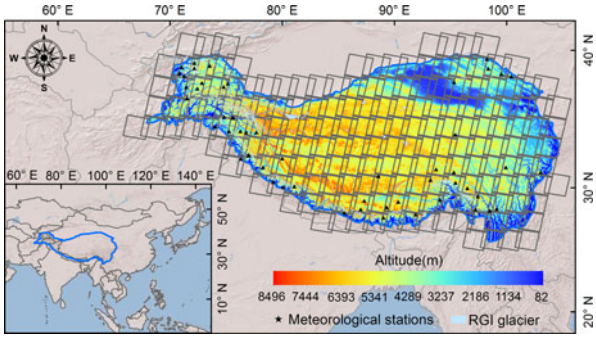

Fig. 1. Location of the Tibet Plateau region. The boundary of Landsat path/rows is showed on the map to showcase the Landsat sidelaps. Glacier outlines are taken from the Randolph Glacier Inventory (RGI v3.2) and the distribution of the 56 meteorological stations is derived from NOAA's National Centers for Environmental Information (NCEI).

turbid over a wide spectral range; this produces heterogeneous reflectance from the lakes and adjacent land surfaces. The varying turbidity and sedimentation characteristics of glacial lakes mean that special techniques are required for automated detection. This paper, for the first time, presents a method for the extraction of glacial lakes that uses an active contour model together with the non-local processing principle, which takes full consideration of the reflectance heterogeneity in satellite images, requiring only local homogeneity in the image. For the large study areas, because of the large data volumes and associated processing required, the Google Earth Engine (GEE), which has open and dense Landsat archive data, was used for the cloud computing [18].

Based on the urgent need for glacial lake area information in high altitude regions and the existing challenges involved in large-scale moderate-resolution glacial lake mapping, the objective of this study are to (1) automatically and efficiently generate glacial lake map in the Tibet Plateau (TP) region for 2015 using Landsat 8 imagery (30 m pixel size); (2) demonstrate the availability of Landsat 8 data for guaranteeing a high quality yearly map of glacial lake on the large scale area like the TP region; (3) explore the unique capabilities of non-local active contour (NLAC) algorithm used for detecting and mapping glacial lakes.

II. The Study Site and Datasets

A. Study Site

The study is the entire TP region, known as the core region of the Earth's third pole, having an average elevation of more than 4000 m above sea level (a.s.l.) and occupying an estimated area of ∼2.50 million km^2 (Fig. 1). The TP contain the largest number of glaciers outside the Antarctic and Arctic. Approximately 36, 800 glaciers are distributed in this area, with an area of about 49, 873.44 km^2 and a total ice volume of 4561 km^3 [19]. They account for 79.5% of the total number of glaciers, 84% of the total glaciated area and 81.6% of the total ice volume in China. These glaciers are the source of many prominent Asian rivers and are largely experiencing shrinkage, which affects the water discharge of large rivers such as the Indus, the Brahmaputra and the Ganges.

This region is one of the most dynamic, fragile, and complex mountain systems in the world [20]. The TP climate is under the combined influences of the East Asian and South Asian monsoons and of the westerlies [21], [22]. The weather is characterized by a thin atmosphere, abundant sunlight, low temperatures with a small annual range and large daily range, and small, unevenly distributed precipitation amounts. Generally, a decrease both in temperature and in precipitation from the south-eastern to the north-western part of the plateau is apparent. For the plateau, the mean temperature of July, as warmest month, varies from 7 °C to 15 °C and from −1 °C to −7 °C in January [23], as coldest month. Average annual temperature is 1.6 °C. Precipitation amounts to about 413.6 mm a year [24], with more than 60–90% falling in the wet and humid summers (June–September) and 10% at maximum in the cool, arid winters (November–February).

B. Datasets

All the Landsat 8 images acquired throughout 2015 belonged to the Level 1 Terrain-corrected (L1T) product and had been archived in the GEE platform as the United States Geological Survey (USGS) Landsat 8 Top-of-Atmosphere (TOA) Reflectance (Orthorectified) collection. These images were also georeferenced with a precision better than 0.4 pixels [25]. To reduce the effect of seasonal variability, images in similar seasons were selected, mainly in autumn and early winters, when glacial lake change is minor after the ablation period of glaciers [26]. A total of 156 path/rows and approximately 3580 scenes were required to cover the whole study area.

Other dataset used included: i) meteorological data provided by NOAA's National Centers for Environmental Information (NCEI) (the locations of meteorological stations are shown in Fig. 1); ii) the Randolph Glacier Inventory (RGI v3.2) [27], based on the RGI data, a buffer distance of 10 km from the nearest glacier termini [5], [28] was adopted to determine the extent of glacial lakes in this study. Glacial lakes farther than 10 km from the nearest glacier termini were excluded due to an assumed weak interaction with current glaciers; and iii) the Shuttle Radar Topography Mission (SRTM) 1 arc-second global data, which was employed to remove the topographical shadows and identify the altitudinal characteristics of mapped lakes. The SRTM data, derived from the National Aeronautics and Space Administration (NASA) and the National Geospatial-Intelligence Agency (NGA) were acquired in 2000 and were provided in geographic coordinates with a 1 arc sec (approximately 30 m) resolution and a high vertical accuracy (root mean square error (RMSE) of less than 8 m) for the area lying between 60° N and 56° S [29].

III. Methodology

The overall methodology developed in this study for detecting glacial lakes over the TP region is given in Fig. 2. The significant advantages of our method are that (1) it is an automated scheme for the extraction of glacial lakes in rugged alpine mountainous areas; (2) it can precisely delineate lake shorelines by taking into account the spatial heterogeneity inside each lake;

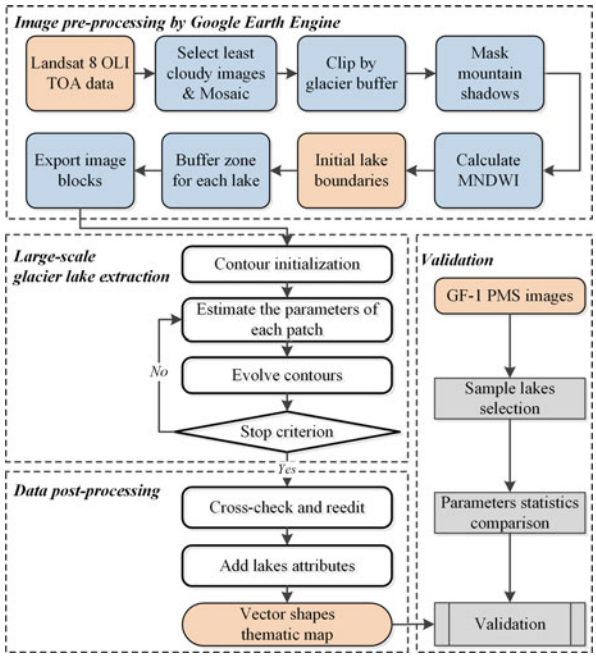

Fig. 2. Flowchart describing the procedure for large-scale glacial lake mapping used in this study. Major modules include pre-processing of Landsat 8 data by GEE, the mapping of each lake by the non-local active contour algorithm, data post-processing (manual cross-checking and reediting) and validation based on sample lakes taken from GF-1 PMS images.

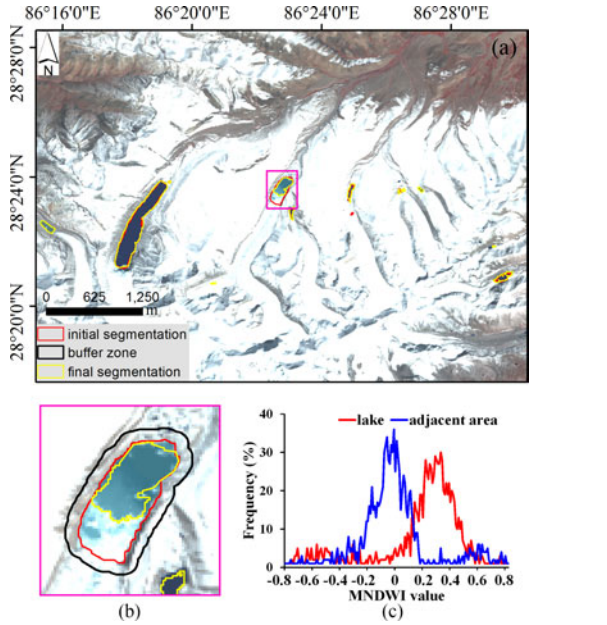

Fig. 3. (a) A false-color composited Landsat 8 OLI image for central Himalayas with band 5 (near infrared), band 4 (red) and band 3 (green) from 9 August 2015. (b) An example of image block for glacial lake extraction using the proposed method. The red contour, the black contour and the yellow contour indicate initial outline obtained by global thresholding, buffer zone of initial outline and the final segmentation result after the regional implementation of NLAC, respectively. (c) The MNDWI frequency histogram for glacial lake and adjacent area of (b).

(3) GEE based cloud computation was used to process a considerable amount of data over large scale area within a short time. Correspondingly, there are four major modules, including pre-processing of the Landsat 8 OLI TOA data by GEE, accurate extraction of individual glacial lake using the NLAC, data post-processing (manual cross-checking and reediting) and validation using sample lakes from higher resolution images. These steps are discussed in detail in the sub-sections below.

A. Image Pre-Processing

All the pre-processing of the Landsat 8 OLI TOA data was conducted using the cloud computing technology available in the GEE platform (https://earthengine.google.org/), which, because it is based on millions of servers located around the world, is able to use parallel computing to make the processing of the large amount of data covering large study areas feasible. In order to ensure complete coverage of the study area, we selected the least cloudy scene from the time series of images for the area covered by each specific path/row. To exclude the effects due to other, non-glacial lakes, the images were clipped using a buffer polygon of glaciers for the study area that was based on the RGI v3.2. Topographic shadows were then masked using knowledge of the sun elevation and azimuth angles at the satellite image acquisition time. In this study, where surface slopes are larger than 10° and shade relief values are less than 0.25 were removed [14, 30].

The normalized difference index of green and short wave infrared band were rightly thought to provide good contrast for detecting glacial lakes in the study area. It is simple to calculate, only using two input bands without tuning parameters. Thus the MNDWI was selected as the image feature to identify the location of glacial lakes. This index was calculated using the equation:

$$\mathrm{MNDWI} = \frac{\rho_{\mathrm{Green}} - \rho_{\mathrm{SWIR}}}{\rho_{\mathrm{Green}} + \rho_{\mathrm{SWIR}}} \tag{1}$$

where ρ_{Green} and ρ_{SWIR} are the TOA values of the green band (0.53–0.59 mm) and short wave infrared band (1.57–1.65 mm) as measured by the Landsat OLI sensor.

After that, the initial glacial lake areas were segmented from the MNDWI imagery by applying a relatively low global threshold of 0.15, which, experimental analysis with many threshold values have shown that 0.15 is suitable to determine almost all of the potential lake areas [14], [31]. The smallest glacial lakes detectable in the Landsat 8 OLI data had an area of 9 pixels, i.e. 0.0081 km^2. However, this still did not give accurate results because the heterogeneous spectral responses of lake water and adjacent land surfaces. A complete example of shoreline extraction from the Landsat 8 imagery is presented in Fig. 3. The water–land boundaries in the lower part of glacial lake in Fig. 3(b) presented mixed reflectance due to a mixture of water and ice from connected glacier. From the MNDWI frequency histogram (Fig. 3(c)), we can find that although the land display obvious discrepancy in value compared with the water, there is a large overlap of MNDWI between them, which demonstrates that it is difficult to use a single threshold to separate the lake from the land directly. Because of this, we define image blocks such that each block contains one lake in a buffer zone of the approximate shoreline (Fig. 3(b)). Taking into account the annual

changes in glacial lake were not too large, a buffer distance of 10 pixels was chosen. These image blocks were then exported from GEE for subsequent regional refinement of the results.

B. Regional Implementation of the NLAC

A NLAC algorithm was used for regional glacial lake mapping based on the images exported from the GEE. The idea here was to partition an image by computing the patch similarity in the image non-locally and then to segment the image using an active contour model. After computing the MNDWI for the images, non-local comparisons between feature patches were used to calculate the active contour energy, which is defined by integrating the interactions between pairs of patches inside and outside the segmented region. Finally, a level set method was used to minimize the non-local energy. Since the level set segmentation is fast for small images but slow for large images, the segmentation speed of whole image blocks can be improved remarkably. Each image block running about three seconds, and the overall runtime for the entire TP region is approximately six hours.

The NLAC model computes the segmentation of an image f as a stationary point of the following optimization problem:

$$\min_{\phi}[E(\phi) + \gamma\, L(\phi)] \tag{2}$$

where ϕ is the level-set function. $E(\phi)$is the energy that measures the similarity between the inside and outside the contour C. $L(\phi)$ is a regularization term and $\gamma > 0$ is a weight parameter used to balance the two terms. As is commonly done in [32], we set $\gamma = 0.1$. The energy $E(\phi)$ is computed in a non-local way as [33], [34]

$$E(\phi) = \iint_{S\times S} G_\alpha(s-t)\cdot d(p_s,p_t)\; d_s d_t + \iint_{S^C\times S^C} G_\alpha(s-t)\cdot d(p_s,p_t)\; d_s d_t \tag{3}$$

where p_s and p_t are the patches centered on pixels s and t, respectively. $d(p_s, p_t) \geq 0$ is a scale metric that accounts for the similarity between patches. S and S^C denote the regions inside and outside the contour C, respectively. $G_a(\cdot)$ is a Gaussian kernel of scale α. The parameter αcontrols the scale of the homogeneity which is required for the segmented object. For simplicity, we set $\alpha = 2$, also the integration inside and outside the contour C is performed using a Heaviside function $H(\phi)$ [35]. Thus, (3) can be transformed as

$$E(\phi) = \iint \rho\left(H(\phi(s)),\; H(\phi(t))\right) \cdot G_\alpha(s-t)\cdot d(p_s,p_t) d_s d_t \tag{4}$$

where ρ is the indicator function defined as $\rho(u,v) = 1 - |u-v|$, which implies that only pairs of pixels for which ϕ has the same sign are considered [36], [37].

The segmentation region is penalized by the length of the contour C:

$$L(\phi) = \int \|\nabla H(\phi(s))\| d_s \tag{5}$$

Combining (2), (4) and (5), the optimization function can be obtained and its minimization can be achieved by using an iterative scheme.

C. Data Post-Processing and Validation

After completing the extraction of the water body boundaries for all the lakes, we cross-checked the results basin by basin to ensure that there were no missing or erroneous lakes. Because Google Earth uses higher spatial resolution images including SPOT 5 (spatial resolution 2.5 m), GeoEye (1.65 m) and Quickbird (2.62 m), the derived lake boundary vector files were then converted to KML format and loaded into Google Earth for visual examination and comparison. According to the acquisition date of Landsat 8 OLI images, the very high spatial resolution images from Google Earth around 2015 were also acquired from September to December. If any errors were identified, the files were edited further using ArcGIS. Specifically, we retained the polygon with the largest area in each block to represent the open water. Errors related to some possible misclassification of small inlands and streams have automatically been eliminated using the platform of ENVI/IDL. Finally, the image acquisition date, lake area, perimeter and centroid are stored as the attributes of shoreline vector files.

In order to achieve robust and quantitative validation of the results, we compared the area and perimeter estimates obtained using the Landsat 8 OLI data with the results derived from GF-1 panchromatic multi-spectral (PMS) images, which were collected during the time from September to December. The classification accuracy of our proposed method was also assessed by calculating kappa coefficients, commission and omission error, etc. The GF-1 satellite was recently launched by China and has a high spatial resolution of 2 m/8 m in the panchromatic/multi-spectral bands. Based on considerations of the amount of work involved and to achieve a suitable sampling number, we selected the glacial lakes from four typical regions as samples – these regions covered the northern Karakoram mountains, western Kunlun mountains, central Himalayas and southeast Tibet. The conditions in the selected test regions ranged from marine to continental glacier and were thus characterized by diverse climatic conditions, physical properties and surrounding environments. The raw PMS panchromatic/multi-spectral images were first ortho-rectificated individually and then processed to create the final 2 m pan-sharpened reference images. The sampled lakes were manually digitized out at the 1:25000 scale using ArcGIS. Glacial lakes in each image were carefully identified and interpreted by experts with knowledge and experience. To make the judgments as objective as possible, we take the comprehensive judgments made by three experts, this ensured consistent examination and high quality control.

IV. Results and Discussion

A. Pattern of Glacial Lakes in Tibet Plateau and Accuracy Assessment

After applying the method proposed in this paper, the spatial distribution of glacial lakes in the TP region was obtained as

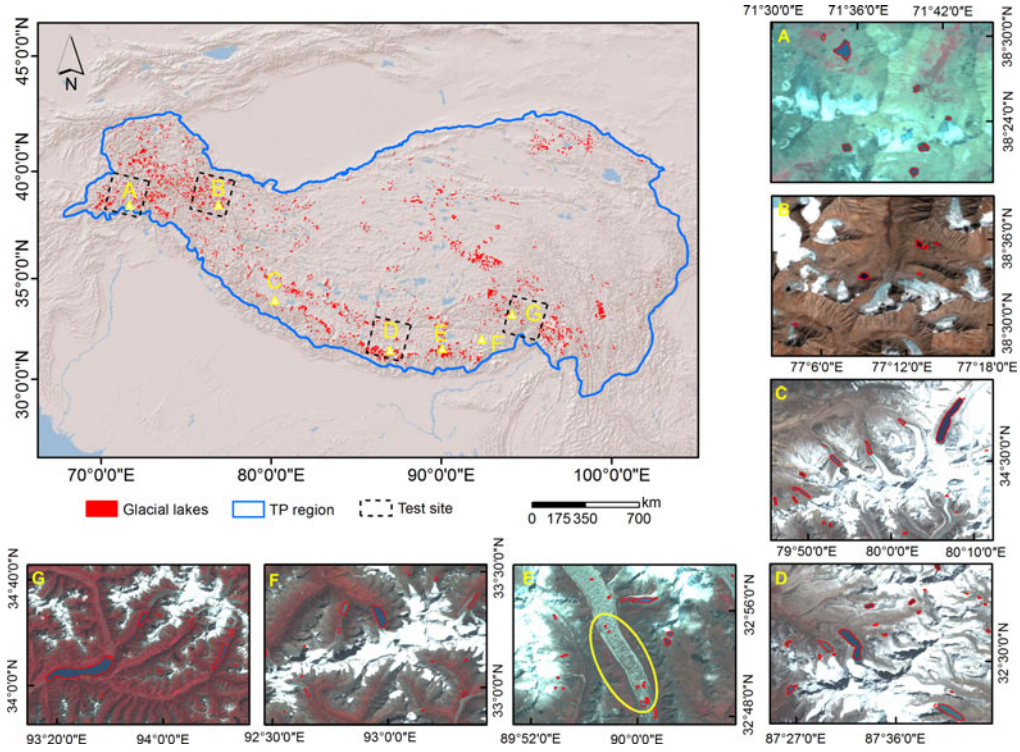

Fig. 4. Distribution of glacial lakes in the TP region in 2015. The surrounding zoom-in maps (Maps A–G) show local detail in different countries and regions, including the northern Karakoram mountains (A), western Kunlun mountains (B), western Himalayas (C), central Himalayas (D), eastern Himalayas (E-F) and southeast Tibet (G). Yellow ellipse in Map E shows some typical supra-glacial lakes in the study area. The black rectangles in the glacial lake map represent the extent of the sampled lakes used for validation.

shown in Fig. 4. As the study area is huge and the glacial lakes are relatively small (many of them less than 0.1 km^2 in area), it is difficult to show all the lake boundaries clearly. Maps A–G show some samples of typical glaciated areas. Generally there are four patterns associated with the glacial lakes. (1) Unconnected glacier-fed glacial lakes, such as those shown in Map A–B, are not connected with their mother glaciers. The occurrence of these lakes is caused by the continuous retreat of debris-free glaciers. (2) Moraine-dammed lakes, such as the lakes in Map C–D, are located next to the glacier terminus and receive melt water directly from their mother glaciers. Such glacial lakes are expanding due to glacier recession induced by global warming [38]. (3) Supra-glacial ponds, such as lakes in yellow ellipse in Map E are formed by surface lowering and increasing glacier stagnation; these lakes have the potential to coalesce into larger lakes where a small glacier surface gradient exists. (4) Glacial lakes that develop around marine glaciers, such as the lakes in Map F and G, have outlines that remain clear and are barely mixed with the glacier snow/ice cover.

These four patterns that occur in the study area suggest that glaciers play a vital role in glacial lake distribution. As this article mainly focuses on yearly lake mapping, time-series analysis of glacial lake changes will be discussed in detail in future papers. Moreover, the combination of annual glacial lake mapping and the resulting multi-temporal information will provide the basis for analyzing the spatial distribution and temporal evolution of glacial lakes and make the identification of potentially dangerous glacial lakes possible.

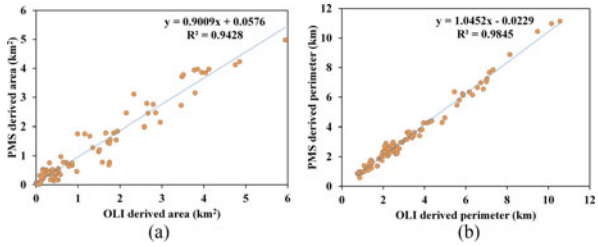

Fig. 5. Comparisons of glacial lake area (a) and perimeter (b) derived from Landsat 8 OLI and GF-1 PMS data for the sampled lakes. R represents the determination coefficient.

To evaluate the matching of the lake boundaries, two measured parameters – area and perimeter were calculated for Landsat 8 OLI and GF-1 PMS, respectively (as shown in Fig. 5). For all the sampled lakes from the four test regions, there is a very high degree of agreement between measured parameters derived from Landsat 8 OLI and GF-1 PMS imagery (the associated R^2 were 0.9428 and 0.9845, respectively). The PMS derived perimeters always showed relatively higher values than the OLI, this is because the higher resolution images could contain more details of lake boundaries. The results of mapping accuracy at each of the four main test sites are summarized in Table I. At all test sites the overall accuracy achieved by our method was higher than 0.90. Taking all accuracy statistics into account, at test site in Southeast Tibet where the glaciers have experienced serious material loss and retreat, our method performed best with the greatest kappa coefficient, overall accuracy,

TABLE I
SUMMARY OF ACCURACY ASSESSMENTS AT THE FOUR MAIN TEST SITES

Test site	Land cover class	User accu.	Produc accu.	Comm. error %	Omi. error %	Kappa	Overall accuracy
Northern Karakoram mountains	Water	96.35	92.84	3.65	7.16	0.93	95.62
	Nonwater	98.42	97.15	1.58	2.85		
Western Kunlun mountains	Water	97.12	91.45	2.88	8.55	0.92	93.21
	Nonwater	98.51	92.74	1.49	7.26		
Central Himalayas	Water	96.86	84.63	3.14	15.37	0.89	91.57
	Nonwater	95.25	99.57	4.75	0.43		
Southeast Tibet	Water	98.91	93.95	1.09	6.05	0.95	97.65
	Nonwater	97.64	98.92	2.36	1.08		

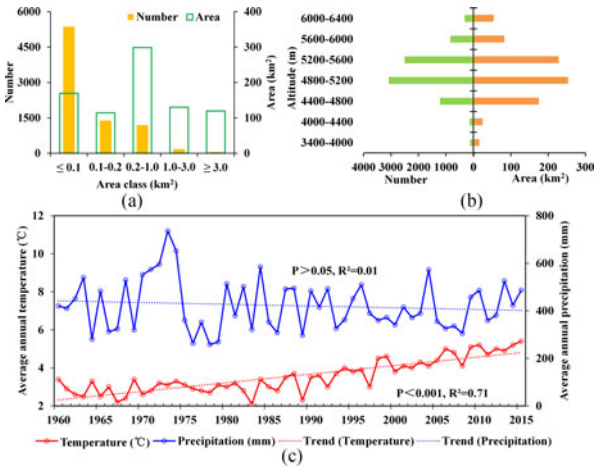

Fig. 6. Statistical analysis of glacial lake in (a) various size classes and (b) elevation gradients for 2015 in the TP region. (c) Mean annual temperature and precipitation during 1960–2015 were recorded at the 56 meteorological stations within the TP region.

greatest water users' accuracy, greatest water producer's accuracy and least commission and omission error. Based on these statistical analyses, it appears, therefore, that the data source and method used to extract glacial lake information over large areas are reliable and robust.

B. Characteristics of Glacial Lake Distribution in Tibet Plateau

The number and area of glacial lakes are spatially heterogeneous, here we have analyzed the characteristics of glacial lake distribution from aspects of various size classes, elevations and their climate forcing before 2015.

tight In total, there were 8215 glacial lakes (832.19 $km^2 \pm 0.012\ km^2$) in 2015 within the study area. In terms of occurrence frequency of the five categories, the majority of the glacial lakes in the TP region are small (area$\leq$0.1 km^2), with this size class comprising nearly 66% of the total number (Fig. 6(a)). Medium-sized (0.1–0.2 km^2 and 0.2–1.0 km^2), large-sized (1.0–3.0 km^2) and giant-sized ($\geq$3.0 km^2) glacial lakes, although less in number, account for 82% of the total glacial lake area. In terms of distribution along the elevation gradients, glacial lakes are distributed within the altitudinal range of 3400–6400 m (Fig. 6(b)), and the majority of them are situated at an elevation of $\geq$4400 m, accounting for 88% and 91% of the total number and area.

The current states of glacial lakes in the TP region definitely have a close relationship with climate change [13], we used the meteorological data from 56 stations to analyze the fluctuations of mean annual temperature and annual precipitation during 1960–2015 (Fig. 6(c)). The mean annual air temperature documents a significant rise at a rate of 0.45 °C/10a during 1960–2015 ($R^2 = 0.71$, $P < 0.001$). In contrast, annual precipitation shows a slight decrease during the same period. The rising temperature was the main climate forcing to glacier shrinkage, which has been reported in many previous studies. Therefore, we estimate that glacial lakes expansion in the TP region mostly by glacier retreat controlled by climate change.

C. Discussion

The experiment of large-scale yearly glacial lake mapping in the TP region using Landsat 8 has been successful, which is largely attributed to the improvement of its sensor and the enhanced image acquisition capability. Fig. 7 shows the observation numbers of individual pixels from Landsat 8 and Landsat 7 in the entire year of 2015. On average, Landsat 8 had an average of 35.2 observations in the study area in 2015 and an average of 21.2 good observations by excluding clouds, snow/ice and cirrus according to the quality assessment band. Moreover, 76% of Landsat 8 pixels had over 30 observations in 2015 and 71% of Landsat 8 pixels had over 15 good observations. While Landsat 7 had an average of 23.6 observations and an average of 12.5 good observations in the study area in 2015. Landsat 8 have much more advantages than Landsat 7 in the data availability in terms of high quality scenes. The higher intensity observations from Landsat 8 in the TP region contribute to a higher temporal resolution of observations and provide more useful information for glacial lake mapping.

Besides, the NLAC approach based on the MNDWI was promising in the TP region. Since regional reflectance heterogeneity of satellite images is a main limitation for accurately extracting glacial lakes, and the MNDWI functions well in spectrally heterogeneous backgrounds [8], the NLAC approach that couple with local information can be applied to refine the initial segmentation of the MNDWI and substantially compensate for the poor spectral contrast. This study furthermore proved this approach reliable for the glacial lake delineation in the complex

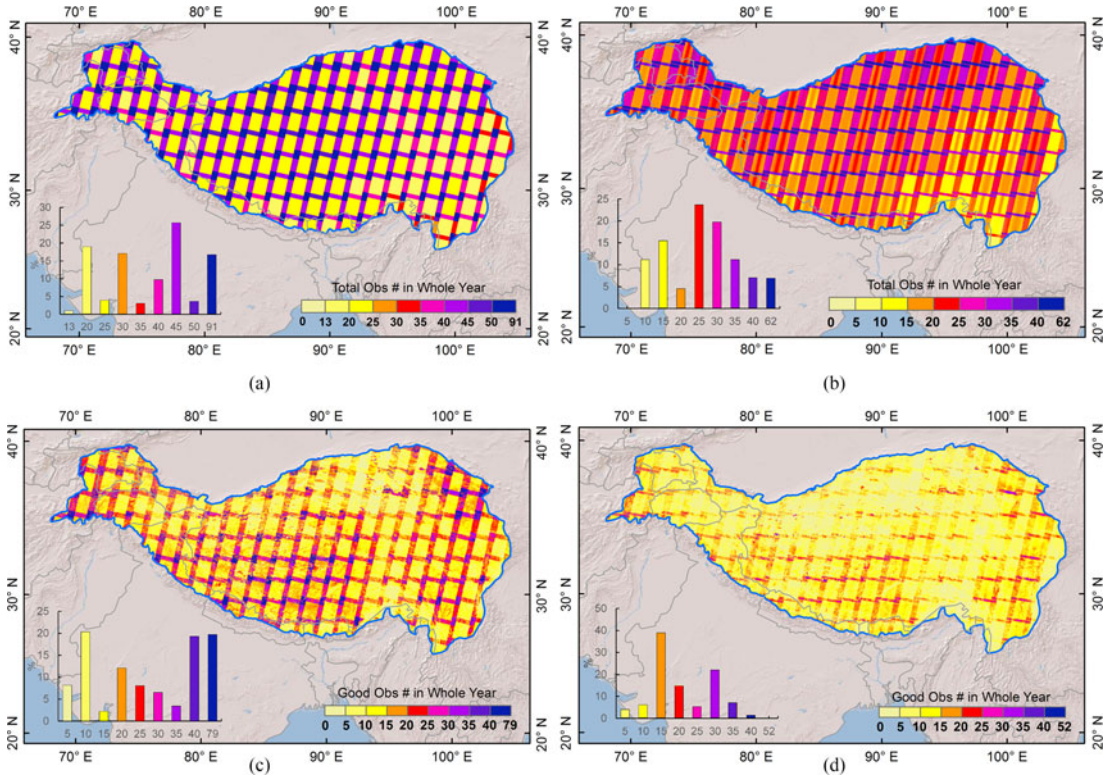

Fig. 7. Availability of time series Landsat images in the study area for 2015. The total observation numbers in the whole year for a) Landsat 8 and b) Landsat 7; the good observation numbers in the whole year for c) Landsat 8 and d) Landsat 7 by excluding clouds, snow/ice and cirrus.

environments in the TP region, and can be extended to other large-scale glaciated area.

V. Conclusion

The preparation of an updated inventory of glacial lakes are an important first step in assessment of GLOF hazard risk. Existing efforts to map glacial lakes are generally focused on local or limited study areas due to the heterogeneous spectral responses involved. Based on the NLAC algorithm and all the available Landsat 8 images from a single year, this study generated a detailed inventory of glacial lakes of the TP region for 2015. The GEE was used for the cloud computing given the huge data size and processing requirement. The MNDWI based NLAC algorithm has been proved robust in mapping various types of glacial lakes. More importantly, this study demonstrate that the Landsat 8 can capture enough quality images during a whole year, which provides an effective support for the high temporal observation requirement of the glacial lake mapping. Validation based on the high-resolution GF-1 PMS images indicated that the glacial lake map that was produced had a high accuracy, with overall accuracy higher than 0.9 at all the test sites. The findings of this study offer an automated scheme of improving the accuracy of detecting glacial lakes over the TP region under different environmental conditions. Further analysis on distribution of glacial lakes verify that climate warming and its induced glacier retreat play a primary role in glacial lake changes. Continued monitoring of glacial lake and detailed analysis of their evolution are the currently urgent task, including by collecting more remote sensing observations and field survey.

References

[1] K. Hewitt and J. Liu, "Ice-dammed lakes and outburst floods, karakoram himalaya: Historical perspectives on emerging threats," *Phys. Geography*, vol. 31, no. 6, pp. 528–551, 2013.

[2] J. J. Liu, Z. L. Cheng, and Y. Li, "The 1988 glacial lake outburst flood in Guangxieco Lake, Tibet, China," *Natural Hazards Earth Syst. Sci.*, vol. 14, no. 11, pp. 3065–3075, 2014.

[3] M. J. Westoby *et al.*, "Modelling outburst floods from moraine-dammed glacial lakes," *Earth-Sci. Rev.*, vol. 134, no. 1, pp. 137–159, 2014.

[4] W. Wang *et al.*, "Rapid expansion of glacial lakes caused by climate and glacier retreat in the Central Himalayas," *Hydrological Process.*, vol. 29, no. 6, pp. 859–874, 2015.

[5] G. Zhang *et al.*, "An inventory of glacial lakes in the Third Pole region and their changes in response to global warming," *Global Planetary Change*, vol. 131, pp. 148–157, 2015.

[6] A. Bhardwaj *et al.*, "Applicability of Landsat 8 data for characterizing glacier facies and supraglacial debris," *Int. J. Appl. Earth Obs. Geoinf.*, vol. 38, pp. 51–64, 2015.

[7] D. P. Roy *et al.*, "Landsat-8: Science and product vision for terrestrial global change research," *Remote Sens. Environ.*, vol. 2014, no. 145, pp. 154–172, 2014.

[8] Y. Yang *et al.*, "Landsat 8 OLI image based terrestrial water extraction from heterogeneous backgrounds using a reflectance homogenization approach," *Remote Sens. Environ.*, vol. 171, pp. 14–32, 2015.

[9] S. K. McFeeters, "The use of the normalized difference water index (NDWI) in the delineation of open water features," *Int. J. Remote Sens.*, vol. 17, no. 7, pp. 1425–1432, 1996.

[10] H. Xu, "Modification of normalised difference water index (NDWI) to enhance open water features in remotely sensed imagery," *Int. J. Remote Sens.,* vol. 27, no. 14, pp. 3025–3033, 2006.

[11] T. Bolch *et al.*, "Identification of glacier motion and potentially dangerous glacial lakes in the Mt. Everest region/Nepal using spaceborne imagery," *Natural Hazards Earth Syst. Sci.*, vol. 8, no. 6, pp. 1329–1340, 2008.

[12] F. Salerno *et al.*, "Glacial lake distribution in the Mount Everest region: Uncertainty of measurement and conditions of formation," *Global Planetary Change*, vols. 92/93, no. 1, pp. 30–39, 2012.

[13] X. Wang *et al.*, "Changes of glacial lakes and implications in Tian Shan, central Asia, based on remote sensing data from 1990 to 2010," *Environ. Res. Lett.*, vol. 8, no. 4, pp. 575–591, 2013.

[14] J. Li, and Y. Sheng, "An automated scheme for glacial lake dynamics mapping using Landsat imagery and digital elevation models: A case study in the Himalayas," *Int. J. Remote Sens.*, vol. 33, no. 16, pp. 5194–5213, 2012.

[15] F. Hu *et al.*, "Transferring deep convolutional neural networks for the scene classification of high-resolution remote sensing imagery," *Remote Sensing*, vol. 7, no. 11, pp. 14680–14707, 2015.

[16] A. Bhardwaj *et al.*, "A lake detection algorithm (LDA) using Landsat 8 data: A comparative approach in glacial environment," *Int. J. Appl. Earth Obs. Geoinf.*, vol. 38, pp. 150–163, 2015.

[17] R. L. Wessels, J. S. Kargel, and H. H. Kieffer, "ASTER measurement of supraglacial lakes in the Mount Everest region of the Himalaya," *Ann. Glaciology*, vol. 34, no. 34, pp. 399–408, 2002.

[18] J. F. Pekel *et al.*, "High-resolution mapping of global surface water and its long-term changes," *Nature*, vol. 540, no. 7633, 2016, Art. no. 418.

[19] T. Yao *et al.*, "Different glacier status with atmospheric circulations in Tibetan Plateau and surroundings," *Nature Climate Change*, vol. 2, no. 9, pp. 663–667, 2012.

[20] J. Bohner, "General climatic controls and topoclimatic variations in Central and High Asia," *Boreas*, vol. 35, no. 2, pp. 279–295, 2006.

[21] F. Maussion *et al.*, "Precipitation seasonality and variability over the Tibetan plateau as resolved by the high Asia reanalysis $*$," *J. Climate*, vol. 27, no. 5, pp. 1910–1927, 2013.

[22] R. Schiemann, D. Lüthi, and C. Schär, "Seasonality and interannual variability of the westerly jet in the Tibetan Plateau region," *J. Climate*, vol. 22, no. 11, pp. 2940–2957, 2009.

[23] Y. Yang *et al.*, "Changes in topsoil carbon stock in the Tibetan grasslands between the 1980s and 2004," *Global Change Biol.*, vol. 15, no. 11, pp. 2723–2729, 2009.

[24] A. Bosch *et al.*, "Potential CO 2 emissions from defrosting permafrost soils of the Qinghai-Tibet Plateau under different scenarios of climate change in 2050 and 2070," *Catena*, vol. 149, pp. 221–231, 2017.

[25] NASA, "Landsat 8 data users handbook," Online, 2016.

[26] Z. Xie *et al.*, "Index for hazard of Glacier Lake Outburst flood of Lake Merzbacher by satellite-based monitoring of lake area and ice cover," *Global Planetary Change*, vol. 107, no. 5, pp. 229–237, 2012.

[27] W. T. Pfeffer *et al.*, "The Randolph Glacier Inventory: a globally complete inventory of glaciers," *J. Glaciology*, vol. 60, no. 221, pp. 537–552, 2014.

[28] X. Wang *et al.*, "Glacier and glacial lake changes and their relationship in the context of climate change, Central Tibetan Plateau 1972–2010," *Global Planetary Change*, vol. 111, no. 12, pp. 246–257, 2013.

[29] M. Kervyn *et al.*, "Mapping volcano topography with remote sensing: ASTER vs SRTM," *Int. J. Remote Sensing*, vol. 29, no. 22, pp. 6515–6538, 2008.

[30] D. J. Quincey *et al.*, "Early recognition of glacial lake hazards in the Himalaya using remote sensing datasets," *Global Planetary Change*, vol. 56, nos. 1/2, pp. 137–152, 2007.

[31] A. Fisher, N. Flood, and T. Danaher, "Comparing Landsat water index methods for automated water classification in eastern Australia," *Remote Sensing Environ.*, vol. 175, pp. 167–182, 2016.

[32] T. F. Chan and L. A. Vese, "Active contours without edges," *IEEE Trans. Image Process.*, vol. 10, no. 2, pp. 266–277, Feb. 2001.

[33] G. Aubert *et al.*, "Image segmentation using active contours: Calculus of variations or shape gradients?" *SIAM J. Appl. Math.*, vol. 63, no. 6, pp. 2128–2154, 2003.

[34] G. S. Xia *et al.*, "Meaningful object segmentation from SAR images via a multiscale nonlocal active contour model," *IEEE Trans. Geosci. Remote Sens.*, vol. 54, no. 3, pp. 1860–1873, Mar. 2015.

[35] H. Wang, T. Z. Huang, and Y. Q. Du, "A global minimization hybrid active contour model with applications to oil spill images," *Comput. Math. With Appl.*, vol. 68, no. 3, pp. 353–362, 2014.

[36] M. Jung, G. Peyré, and L. D. Cohen, "Non-local active contours," *Siam J. Imaging Sci.*, vol. 5, no. 3, pp. 255–266, 2012.

[37] T. Brox and J. Weickert, "Level set segmentation with multiple regions," *IEEE Trans. Image Process.*, vol. 15, no. 10, pp. 3213–3218, Oct. 2006.

[38] S. S. Thompson *et al.*, "A rapidly growing moraine-dammed glacial lake on Ngozumpa Glacier, Nepal," *Geomorphology*, vol. 145, no. 4, pp. 1–11, 2012.

Fang Chen received the B.Sc. degree in science of environment from the Northwestern Polytechnical University, Xi'an, China, in 2003 and the Ph.D. degree in cartography and geographic information system from the Institute of Remote Sensing Applications, Chinese Academy of Sciences (CAS), Beijing, China, in 2007.

He is a Professor at the Institute of Remote Sensing and Digital Earth, CAS. He conducts interdisciplinary work combining, remote sensing, ecology, and other fields of study to assess spatial patterns of disaster risk. He is an expert on wildfire, employing satellite remote sensing to assess the characteristics, behaviour and severe effects of fire in semiarid rangeland and temperate forests that are inherent to current systems of human land-use and management. He has completed numerous research projects since he started his academic career and is a blossoming scholar who has a splendid record publication. He has published more than 30 original research articles in peer-reviewed, internationally recognized journals and one patent. He has been involved in numerous professional activities, and speaks worldwide on a broad range of Earth observation and disaster issues. In 2011, he was elected to the CAS "Hundred Talent Program" and he is currently serving as Executive Deputy Director of the CAS-TWAS Centre of Excellence on Space Technology for Disaster Mitigation (SDIM), coordinating and involving in multiple collaborative projects related to capacity building in disaster risk management in developing countries.

Dr. Chen is selected as a TWAS Young Affiliate Fellow in 2014.

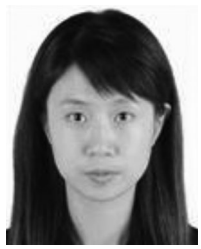

Meimei Zhang received the B.S. and M.S. degrees in cartography and geographic information sciences from China Agricultural University, Beijing, China, in 2012, and the Ph.D. degree at the Institute of Remote Sensing and Digital Earth, Chinese Academy of Sciences, Beijing, China, in 2016.

She is currently an Assistant Researcher with the Institute of Remote Sensing and Digital Earth, Chinese Academy of Sciences. Her research interests include the retrieval of disaster characteristic parameters and its application.

Bangsen Tian received the B.S. degree in surveying and mapping engineering from Wuhan University, Wuhan, China, in 2005 and the Ph.D. degree in cartography and geographic information system from the Institute of Remote Sensing Application, Chinese Academy of Sciences, Beijing, China, in 2010.

He is currently an Associate Researcher with the Institute of Remote Sensing and Digital Earth, Chinese Academy of Sciences. His research interests include synthetic aperture radar image processing and modeling scattering of electromagnetic waves for microwave remote sensing application

Zhen Li received the B.S. degree in photogrammetry and remote sensing from Wuhan University, Wuhan, China, in 1988, and the Ph.D. degree in natural geography from the Cold and Arid Regions Environmental and Engineering Research Institute, Chinese Academy of Sciences, Lanzhou, China, in 1998.

He is currently a Professor and the Director of the airborne remote sensing center at the Institute of Remote Sensing and Digital Earth, Chinese Academy of Sciences, Beijing, China. He is the author of more than 60 journal papers and has published two books in collaboration with others. His current research interests include microwave remote sensing, global change, and environment and disaster remote sensing.